ACS OMEGA

http://pubs.acs.org/journal/acsodf

Article

Electric Conductivity Study of Porous Polyvinyl Alcohol/Graphene/Clay Aerogels: Effect of Compression

Vicente Compañ,* Andreu Andrio, Jorge Escorihuela, Josua Velasco, Alejandro Porras-Vazquez, and Jose Gamez-Perez*

Cite This: *ACS Omega* 2022, 7, 37954−37963

Read Online

ACCESS | Metrics & More | Article Recommendations

ABSTRACT: In this work, poly(vinyl alcohol) (PVOH)/graphene (GN) oxide/clay aerogels were prepared using montmorillonite (MMT) and kaolinite (KLT) as fillers. This work paves the way for the development of aerogels filled with MMT or KLT with high conductivity. The mechanical properties of the polymer/clay aerogels are enhanced by incorporating GN into these systems. These composite materials have an enhanced thermal stability, and the combination of PVOH and GN leads to interconnected channels which favored the conductivity when a clay (MMT or KLT) is added to the mixed PVOH/GN matrix. However, after compressing the samples, the conductivities drastically decreased. These results show that the design of solid MMT/GN and KLT/GN composites as aerogels allows maximizing the space utilization of the electrode volume to achieve unhindered ion transport, which seems contrary to the general design principle of electrode materials where a suitable porous structure is desired, such as in our uncompressed samples. These findings also demonstrate the potential of these materials in electrodes, sensors, batteries, pressure-sensing applications, and supercapacitors.

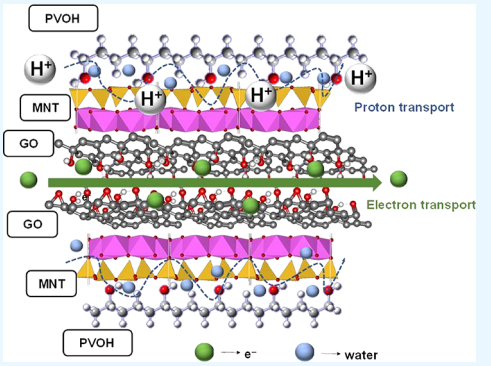

INTRODUCTION

Supercapacitors are materials that combine the properties of batteries and conventional capacitors and are an emerging technology that can help fill a crucial gap in today's energy storage needs.[1] Thus, improving the energy density of supercapacitors is critical for its widespread use. The energy density of this material is calculated using the equation $E = 1/2 \cdot C \cdot V^2$, where E is the energy density, C is the cell capacitance, and V is the cell voltage. As inferred from this equation, the cell voltage plays an important role in enhancing energy density and there is one approach to broaden the cell voltage. It is to use organic or ionic liquid electrolytes which raise the voltage. However, the toxicity, high-cost, and the working temperature limitations of organic electrolytes and ionic liquid electrolytes make this approach unfavorable.[2] For these reasons, good materials to achieve high capacitance is to create porous nanostructures which provide a sufficient interface between electrode materials and the electrolyte, leading to fast energy conversion in both faradic and non-faradic process.[3] In this context, graphene (GN) has been highlighted as an option for its outstanding characteristics, such as its large surface area (2650 m^2/g), its processability in solution, its high electrical conductivity, its excellent mechanical and thermal properties, and its high electrochemical stability.[4,5] In addition, this material has already found applications in the areas of composites, nanoelectronics, energy storage, sensors, catalysis, and biomedicine.[6] It is therefore an interesting material for the manufacture of supercapacitors, especially in composites. However, the most used 3-D materials include hydrogels,[7] aerogels,[8] and kitchen sponge. Of all of them, aerogels are the most promising because (i) hydrogels may lack mechanical robustness and cannot provide fast transport of electrolyte and (ii) aerogels can be very conductive when doped with suitable materials.

Aerogels are well-known materials that were invented back in 1931 by Kistler,[9] when the first aerogels utilizing a novel sol−gel and drying process was synthesized. This is one of the lowest density materials known typically exhibiting bulk densities ranging from 0.005 to 0.1 g/cm^3, and they attracted a lot of attention as quite revolutionary solid-state materials due to this property and others such as their high specific surface areas, high porosities, and low thermal conductivities. In addition to the use of silica, aerogels based on GN, clay, carbon nanotubes, and polymers have also been made, giving

Received: August 10, 2022
Accepted: September 12, 2022
Published: October 12, 2022

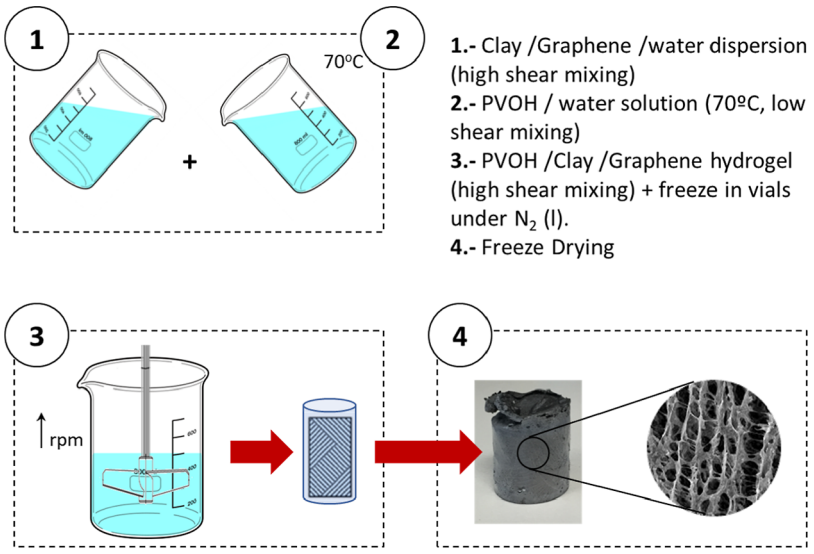

Figure 1. Schematic representation of the preparation of aerogels.

them interesting new properties and increasing their range of applications.[10,11]

Poly(vinyl alcohol) (PVOH) is a hydrophilic and water-soluble polymer which constitutes an ideal candidate for fabricating polymer aerogels because of its low toxicity, good chemical stability, and favorable mechanical properties.[12,13] Due to its properties, PVOH-based materials and aerogels have been efficiently used in many fields, such as acoustics,[14,15] reinforcers,[16] oil spillage applications,[17] antibacterial agents,[18] superabsorbents,[19] pressure-sensing applications,[20,21] among others. As such, there is an increasing interest in developing novel organic PVOH-based aerogels with superior properties.

Clay aerogels are typically fabricated by freeze-drying and they are very fragile due to the weak interactions between clay clusters within layered structures preventing their use in practical applications. Therefore, water-soluble or water-dispersible polymers are introduced to improve the mechanical strength and integrity of the material through the enhancement of the load transfer characteristics for clay-filled polymer composites.[22,23] Montmorillonite (MMT) and kaolinite (KLT) are two of the most used clays in the world of nanocomposite research and development because in the presence of water, these clays are swellable and can exchange cations present in their structure for other cations, making it a relatively easy clay to modify chemically. On the one hand, MMT and KLT are natural, abundant clay minerals composed of silicate aluminate sheets with strong in-plane chemical bonds, which display highly porous structures and excellent absorption properties.[24,25] Therefore, MMT and KLT are considered as two of the most appropriate raw materials for preparing inorganic aerogels with good mechanical strength, thermal stability, and flame retardation.[26]

In this work, the electrical and thermal properties of different aerogels based PVOH/GN doped with MMT and KLT, named PVOH/GN/MMT and PVOH/GN/KLT, respectively, are studied with the aim of developing good electrodes and supercapacitors with excellent properties that make them useable in a wide range of applications and can help to meet energy storage needs. Their properties were investigated in their original and compressed forms. Our findings show that after compressing the samples, the conductivity is drastically decreased in comparison with the high conductivity observed for the uncompressed aerogels.

EXPERIMENTAL SECTION

Materials. Polyvinyl alcohol (PVOH, M_w 31000−50000) and sodium MMT were purchased from Sigma-Aldrich. Natural KLT was supplied by Arciblansa (Alcora, Spain). GN (1% oxygen) has been purchased from XG Sciences, Inc (Lansing, MI, USA). All materials were used as received, without any further treatment. Deionized water (DI) was used in all experiments.

Preparation of Aerogels. PVOH was initially dissolved in half of the DI required for the aerogel using a magnet stirrer and heating at 70 °C during 30 min. The MMT or KLT and GN were also dispersed in water, stirring with high shear using hand blender (Braun Minipimer, Germany) for 5 min at room temperature, ensuring a homogeneous dispersion. Then, the dissolved PVOH was incorporated to the MMT/GN or KLT/GN dispersion and mixed at high shear, letting the resulting gel to settle to avoid trapped bubbles and to obtain a homogeneous suspension. After mixing, the solution was poured into cylindrical vials where they were frozen in an ethanol/solid carbon dioxide bath (−70 °C) for 15 min. These vials were placed in the refrigerator for 1 day to relieve internal stresses and then placed in the freeze-dryer for 48 h until the dry porous solid was obtained. These samples were freeze-dried using a Telstar Serie LyoQuest −85 lyophilizer, with the shelf temperature set to 35 °C, and the pressure set to under 0.05 mbar, until the dry porous solid was obtained. The process for obtaining the aerogels is schematized in Figure 1. Table 1 summarizes the aerogels prepared.

Characterization. The aerogel densities were calculated by measuring the mass and dimensions using an analytical balance and a digital caliper. Every composition was tested with four samples. Scanning electron microscopy (SEM) was conducted on a JEOL 7001F scanning electron microscope (Tokyo, Japan) with a hot cathode FEG electron gun (0.1−30 kV), installed together with a digital image acquisition system. The aerogel samples used for the micrographic study were obtained by wire-cutting the frozen samples to preserve the microstructure by performing a fragile fracture. The thermogravi-

https://doi.org/10.1021/acsomega.2c05123
ACS Omega 2022, 7, 37954−37963

Table 1. Sample Composition and Nomenclature

nomenclature	PVOH wt [%]	MMT wt [%]	KLT wt [%]	GN wt [%]
PVOH/MMT	5.0	5.0		
PVOH/KLT	5.0		5.0	
PVOH/GN	5.0			5.0
PVOH/GN[a]	5.0			5.0
PVOH/GN/MMT	7.5	2.5		5.0
PVOH/GN/MMT[a]	7.5	2.5		5.0
PVOH/GN/KLT	7.5		2.5	5.0
PVOH/GN/KLT[a]	7.5		2.5	5.0

[a]Indicates compressed samples.

metric analysis (TGA) of the MMT/PVOH/GN and KLT/PVOH/GN aerogels was performed on a Mettler Toledo TG-STDA, model TGA/STDA851 e/LF/1600. The thermal cycle applied was an initial isotherm of 50 °C for 10 min and a subsequent temperature sweep until reaching 900 °C, at a constant heating rate of 10 °C/min. All the tests were carried out in an inert atmosphere of nitrogen gas. Differential scanning calorimetry (DSC) analysis of the aerogel samples was carried out using a PerkinElmer DSC model DSC-7. Stress−strain tests of the aerogels were carried out using a Shimadzu AG-X universal testing machine with suitable chucks to compress the samples. The tests were carried out at room temperature. The specimens tested have a cylindrical geometry, with a diameter and height of 20 mm, respectively, so that a ratio $L/D = 1$ is followed. The tests were carried out at a compression speed of 5 mm/min with a load cell of 500 kN. The maximum applied force was set at 80% of the total load. For each formulation, at least two replicates were performed, and the results averaged. Figure 2 shows the aspect

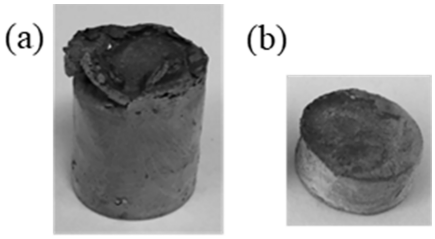

Figure 2. Picture of PVOH/GN/MMT (a) uncompressed and (b) compressed aerogel.

of a PVOH/GN/MMT aerogel as pulled out from the vial (a) and the specimen after compression test (b). The diameter remained the same because compression only produced a collapse in the porous structure. Electrochemical impedance spectroscopy (EIS) measurements were performed on 5 mm height discs, which were cut from compressed and non-compressed samples. EIS measurements were carried with a frequency window of $10^{-1} < f < 10^{7}$ Hz. The experiments were performed with 100 mV amplitude using a Novocontrol broadband dielectric spectrometer (Hundsangen, Germany) integrated by an SR830 lock-in amplifier with an alpha dielectric interface. Experimentally, 100 mV was chosen as the appropriate voltage to attain a linear response. Thus, two gold electrodes were attached to both sides of the sample synthesized in a sandwich cell configuration. The EIS measurements were performed following reported procedures.[27,28] Briefly, the assembled membrane-electrode was annealed in the Novocontrol setup under an inert N_2 atmosphere. The measurements, in case of the aerogels PVOH/GN, were carried out in two temperature cycles wherein, in the first cycle, the temperature was raised from ambient temperature to 220 °C and then lowered to 20 °C, while in the other cycle, the temperature was raised from 20 to 220 °C. For the samples X/PVOH/GN (X = MMT and KLT), for the first cycle, the temperature was raised from ambient temperature to 120 °C and then lowered to 20 °C. After in a second cycle, the temperature was carried out from 20 to 120 °C. All of them in steps of 10 °C with the measurement of the dielectric spectra.

RESULTS AND DISCUSSION

In our efforts for synthesizing polymer−clay aerogels, we found that the optimal performance in terms of mechanical properties was found for those aerogels prepared with equal ratios of polymer and clay. When the polymer fraction was lower, the aerogels were not stable after freeze-drying, becoming a dusty material difficult to handle. On the other hand, when the polymer ratio was higher, the aerogels would not keep its shape during freeze-drying, shrinking, and increasing its final density. When observing the structure in SEM, we found that the clay was charged by electron irradiation. This finding led us to consider a good hypothesis to use the ability of the laminar clays to trap electrons with conductive GN layers to build supercapacitors with a high surface aspect. After assaying different ratios of PVOH/GN in the preparation of aerogels (without any clay), the best conducting performances were obtained with aerogels having 5% of PVOH and 5% of GN.

Another phenomenon that caught our attention was that after compressive testing of aerogels, the resulting specimens held good appearance and increased hardness. This finding can be attributed to a pore reduction after compression, whereas the active surface should be kept very high. Hence, it was worth to study in detail the properties of the compressed aerogels in case that they could show similar active surface in a more compact distribution.

Compression Testing of Aerogels. The apparent densities (ρ_{ap}) for the samples prepared in this study are listed in Table 2. The PVOH/GN aerogel with the lowest

Table 2. Experimental and Theoretical Apparent Densities (ρ_{ap})

sample	experimental ρap (g/cm^3)	theoretical ρ_{ap}(g/cm^3)
PVOH/GN	0.124 ± 0.008	0.10
PVOH/MMT	0.101 ± 0.001	0.10
PVOH/KLT	0.150 ± 0.002	0.10
PVOH/GN/MMT	0.164 ± 0.008	0.15
PVOH/GN/KLT	0.194 ± 0.004	0.18

shrinkage and the lowest solid concentration, showed the lowest apparent density (ρ_{ap} = 0.124 g/cm^3). As expected, sample densities increased with the increase in solid content. Aerogels with bulk densities close to the theoretical ones were obtained. However, it was not possible to reach the theoretical bulk densities, with some contraction being noted in the samples after freeze-drying, thus the value of the bulk density of the material increases slightly.

The compressive behaviors of aerogels composed of PVOH, GN, and clays are shown in Figure 3. The mechanical properties of aerogels can be influenced by many factors including composition, microstructure, and apparent densities.

https://doi.org/10.1021/acsomega.2c05123
ACS Omega 2022, 7, 37954−37963

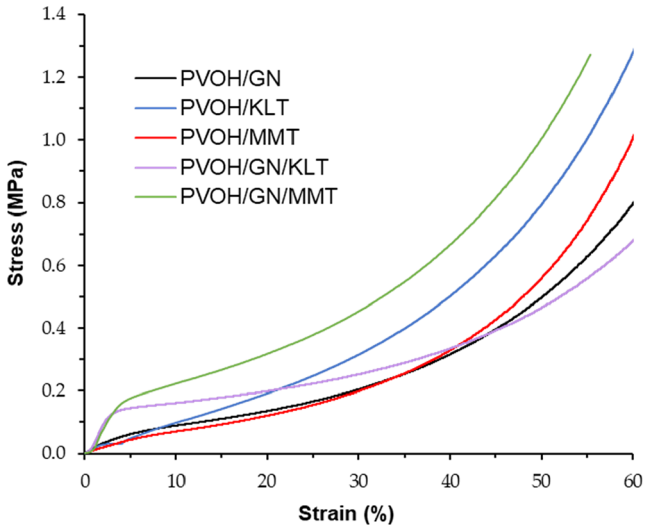

Figure 3. Stress−strain curves of the PVOH/GN/clay aerogels.

As inferred from Figure 3, the compression behavior of most polymer/clay aerogels is analogous to that of polymeric foams commonly used in industry.[29] This figure shows the different stress−strain curves for each of the samples, showing some appreciable differences in the initial slope or in the maximum stress reached at the end of the test. However, the samples did not reach complete failure as a maximum stress of 400 N was reached for machine safety.

The stress−strain curve is generally characterized by three distinct phases, each of them attributed to a particular phenomenon. However, in our samples two differentiated sections were observed. The first one was characterized by an initial section of linear elasticity at low stresses, which corresponds to an elastic region due to the deformation of the pores present in the rigid foam of the aerogels, related with the polymer fraction and its adhesion to the fillers. This region was followed by another where the material densification phenomenon was observed, in which cells touch each other, leading to a sharp increase in stress without a usual observation of a plateau due to the collapse of the cells, as observed in pure clay foams, where systematic fracturing of the walls of the foam itself occurs before ending with a densification. In this region around 10% strain, the connections between the GN/clay sheets undergo brittle fracture and a gradual increase in stress is observed. At rupture stress σ_R, (around 30−35%) the phenomenon of densification occurs in the compressed sample, where the space between lamellae and faces is reduced, producing a sharp increase in the stress experienced. On the other hand, it can be observed how the compression behavior of the PVOH/GN/clay aerogels is a typical behavior similar to that of a polymer nanocomposite.[30] It can be contrasted how initially a stage of linear behavior can be seen corresponding to the elastic deformation of the PVOH/GN/clay lamellae. When moving to zone II, the connections between the GN/clay sheets undergo brittle fracture and a gradual increase in stress is observed. At stress σ_R, the phenomenon of densification occurs in the compressed sample, where the space between lamellae and faces is reduced, thus producing a sharp increase in the stress experienced.

From the curves in Figure 3, the different parameters for the mechanical characterization of the aerogels were determined (Table 3). Thus, Young's modulus "E", specific rigidity (E/ρ), yield strength (σ_y), and stress (σ_R) have been analytically determined, showing the transition between the plateau and the densification zone. The stress at a strain of ε = 30% (σ_{30}), which corresponds to similar conditions of use to which the material in question will be exposed in most industrial applications.

There is a tendency for the aerogels to have higher elastic modulus when the composition contains MMT compared to those containing KLT. Likewise, the same effect is observed for the values of the elastic limits studied, which are always higher with MMT than with KLT. Comparing the different mixtures, replacing the clay with GN causes the compressive modulus E of the aerogel to decrease compared to pure clay aerogels. On the other hand, the inclusion of GN in the compositions of pure clay aerogels has the effect of increasing the specific rigidity as well as the mechanical strength of the aerogels.

The observed high stiffness of the aerogel can be attributed to the fact that the PVOH forms a strong interconnected network of filaments covering and linking the different layers of clay and GN.[31] In this way, the polymer can transfer the applied stresses more efficiently, which results in higher strength and stiffness values. Furthermore, the same effect has been observed with the clay content due to the interaction between the clay particles and the GN. Indeed, an increase in the amount of clay or GN would lead to a decrease in the mobility of the polymer chains as they will be confined in the galleries of the clay/GN platelets. In general, it has been observed that the composition with the highest Young's modulus and yield strength is the one containing 7.5% of PVOH, 5% of GN, and 2.5% of MMT.

Morphology. SEM was used to investigate the aerogel morphologies and the relationship between the structure and its properties. Representative images of the structure generated in the aerogels are displayed in Figure 4. As the ice crystals nucleate and grow, the clay, GN, and polymer molecules are pushed out of the crystal structure to the interstitial regions in between. After freeze-drying, this structure reproduces the template of the ice crystals, being stabilized by the polymer, which precipitates in the surface of the fillers, holding everything together. In our case, the aerogels that incorporated GN showed larger interlaminar spaces, with a more defined structure. We think that GN may play a role in stabilizing these

Table 3. Mechanical Properties of PVOH/GN/Clay Aerogels[a]

sample	E (MPa)]	E/ρ(J/g)	σ_y (MPa)	σ_{30} (MPa)	σ_R (MPa)
PVOH/MMT	1.9 ± 0.1	18.5 ± 0.2	0.06	0.29	0.47
PVOH/KLT	0.9 ± 0.1	6.2 ± 0.1	0.09	0.29	0.44
PVOH/GN	1.4 ± 0.2	11.4 ± 0.2	0.20	0.47	0.54
PVOH/GN/MMT	5.7 ± 0.1	35.5 ± 0.4	0.06	0.20	0.29
PVOH/GN/KLT	2.4 ± 0.1	12.2 ± 0.3	0.05	0.20	0.36

[a]Young's modulus (E), specific rigidity (E/ρ), yield strength (σ_y), stress at a strain of ε = 30% (σ_{30}), and stress (σ_R).

https://doi.org/10.1021/acsomega.2c05123
ACS Omega 2022, 7, 37954−37963

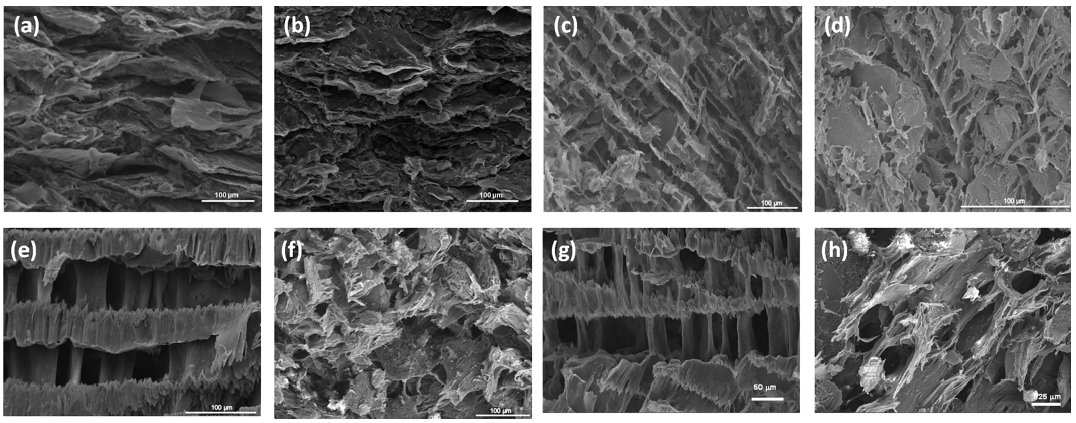

Figure 4. SEM images of aerogel samples: (a) PVOH/MMT, (b) PVOH/KLT, (c) PVOH/GN (d) PVOH/GN* (compressed) (e)PVOH/GN/MMT, (f) PVOH/GN/MMT* (compressed), (g) PVOH/GN/KLT, and (h) PVOH/GN/KLT* (compressed).

layers because they showed significant larger spacing, and the structure was more resilient when it was cut for SEM observation. Table 4 shows the average interlaminar spacing observed in the prepared aerogels.

Table 4. Interlaminar Spacing in Aerogels after SEM Observation

sample	interlaminar space (mm)
PVOH/MMT	25
PVOH/KLT	24
PVOH/GN	30
PVOH/GN/MMT	58
PVOH/GN/KLT	56

Figure 4 shows typical house of cards aerogel structures, which is a lamellar structure caused by ice growth during the freezing stage.[32] This structure is obtained because during freeze-drying, sublimation of the ice occurs, preserving the lamellar structure previously created during freezing. PVOH appears to cover the different clay/GN lamellas. Indeed, this can be explained by the fact that PVOH exhibits high interactions, forming a polymer network throughout the aerogel microstructure, forming hydrogen bridges. PVOH has not only been found covering the clay/GN lamellas but has also appeared interconnecting them through an extensive and dense network of filaments. As far as the growth of the layers of lamellae is concerned, they grow radially from the center of the sample. Indeed, this phenomenon has been observed previously by Van Olphen and co-workers in their study on polymer/clay aerogels.[33]

The combination of the clay and GN seems to favor unusual very well-defined structure cases (Figure 4a,b), not commonly seen on other works of aerogels with GN oxide. A look at the PVOH/GN microstructure (Figure 4c) shows that GN platelets are not only placed parallel to each other with this process in the main direction of crystal growth but also making supports holding the stack. When the clays are added, the same behavior appears, but in these cases, the lamellar structure is thicker and the columns that hold them apart are bigger (Figure 4e,g). Thus, the resulting morphology can be considered as more ordered, with solid connectors between the layers.

After compressive stress, the lamellar structure collapses, finding that the pore size is reduced. Furthermore, it is not possible to find the print of the lamellar structure that was present in the uncompressed samples (Figure 4f,h).

Thermal Stability and Degradation Mechanism. The thermal stabilities of the aerogels in this study were investigated by TGA (Figure 5). These tests show the typical

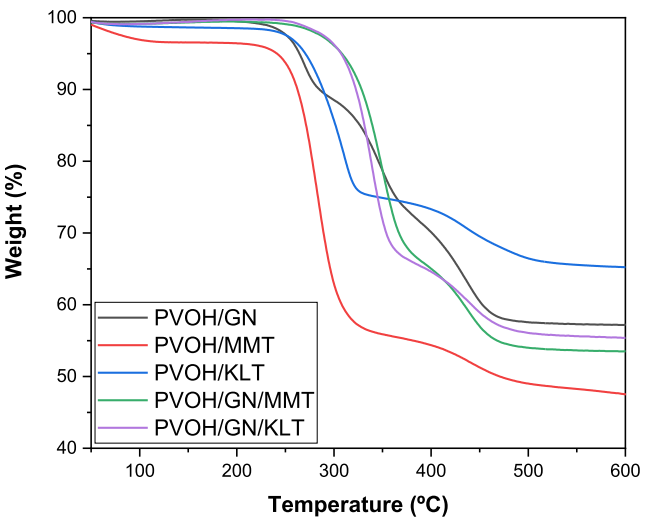

Figure 5. TGA curves of PVOH-based aerogels under a N_2 atmosphere.

thermal degradation processes associated with the components: water loss (associated with MMT), polymer degradation (PVOH), and clay dehydroxylation in MMT and KLT.[34]

Typically, in MMT aerogels, a weight loss around 100 °C can be observed, attributed to the evaporation of the water present in the internal galleries of the aerogel (first stage). In a second stage, from 250 to 350 °C, the curves show a sharp drop, attributable to the degradation of PVOH with the generation of volatile products, such as water, from the dehydration of the polymer chain, as well as other volatiles that are also generated from the degradation of the polymer chain, such as acetaldehyde and ketones.[35] A third stage (350−450 °C) corresponds to further degradation of PVOH, leaving a residue, which can be considered as graphitized PVOH; also, dihydroxylation of the clays may occur at this temperature range.

The main parameters extracted from the TGA are listed in Table 5. Herein, $T_{5\%}$ indicates the temperature at which 5%

https://doi.org/10.1021/acsomega.2c05123
ACS Omega 2022, 7, 37954−37963

Table 5. Degradation Temperature Experienced by the Manufactured aerogels, and Parameters Obtained From the TGA Study of the Fabricated Aerogels

sample	$T_{5\%}$ (°C)	T_{d1} (°C)	T_{d2} (°C)	residue (%)
PVOH/GN	264	347	431	57.2
PVOH/MMT	244	283	443	47.6
PVOH/KLT	268	312	435	65.0
PVOH/GN/MMT	305	337	437	55.5
PVOH/GN/KLT	305	348	436	53.5

degradation of the compound has occurred and it is related with the initiation of thermal degradation. T_{d1} and T_{d2} correspond to temperature of the peaks for each curve of the DTG diagram, at which degradation occurs at maximum rate for the second and third stage, respectively. Finally, the percentile residual shows the amount of undegraded compound remaining at the end of the temperature cycle.

It is worth mentioning that GN alters the signal of PVOH degradation, as evidenced in the shape of the TG curve, in contrast with PVOH/MMT. Furthermore, aerogels with a single loading element (either GN, KLT, or MMT) start to degrade ($T_{5\%}$) earlier than aerogels with clay and GN together. This effect can be attributed to the addition of GN, especially in combination with the clays, which hinders the degradation of the polymer. Hence, it can be reasonably hypothesized that volatiles get trapped on the GN surface, thus delaying the signal of mass loss. The fact that PVOH/GN/MMT and PVOH/GN/KLT showed such a relevant retardation in peak temperature (ca. 60 °C with respect to PVOH/MMT) can be attributed to the trapping of PVOH between the MMT sheets and GN platelets. That would explain the deviation of the degradation temperatures toward higher values.

During the last stage of degradation, some differences in the behavior of the compounds can be observed. They displayed the highest degradation rates for aerogels containing GN and clay together. At the end of the thermal cycle, the aerogel samples show a residue around 55% of the original mass, values that are consistent because a 50−50% polymer to filler ratio was set, the filler being the clay and/or the GN used. Only the PVOH/KLT aerogel ended up with a residual of 65%, possibly due to the flame-retardant effect of the clay.

Conductivity Analysis. The conductivity of the aerogels PVOH/GN, PVOH/GN/KLT, and PVOH/GN/MMT, was measured by EIS following two different procedures. (a) The aerogel samples sandwiched between the two gold electrodes and, (b) the samples with KLT and MMT were compressed before to be sandwiched. The results of the conductivity obtained versus frequency, in all the range of temperatures under study (20−120 °C) is shown in Figure 6. Both cases were compared to be the effect of the clay (KLT and MMT) on the structure of the PVOH/GN aerogel when the samples maintain the same configuration that has been imposed by their synthesis and preparation with respect to the state of the samples after they have been compressed.

A close inspection of Figure 6 shows a large difference in the behavior between the values obtained for the uncompressed and compressed samples without compression. In this regard, uncompressed samples displayed a pure conductor behavior, where conductivity remains practically constant along all the frequency range and increases as the temperature increases. Furthermore, the incorporation of 5% of MMT and KLT produced an increase of conductivity in comparison with the sample PVOH/GN in all the interval of temperatures studied, being around 500-fold higher in case of PVOH/GN/KLT and 1500-fold higher when using MMT as the doping agent. This effect is less pronounced as temperature increases.

However, after compressing the samples, the conductivities drastically decreased. These findings differ from previous studies of GN-embedded polymer aerogels.[36,37] A close inspection of the panels showed in Figure 6 shows conductivities varying from 10^{-4}, 0.14 and 0.055 S/cm at 20

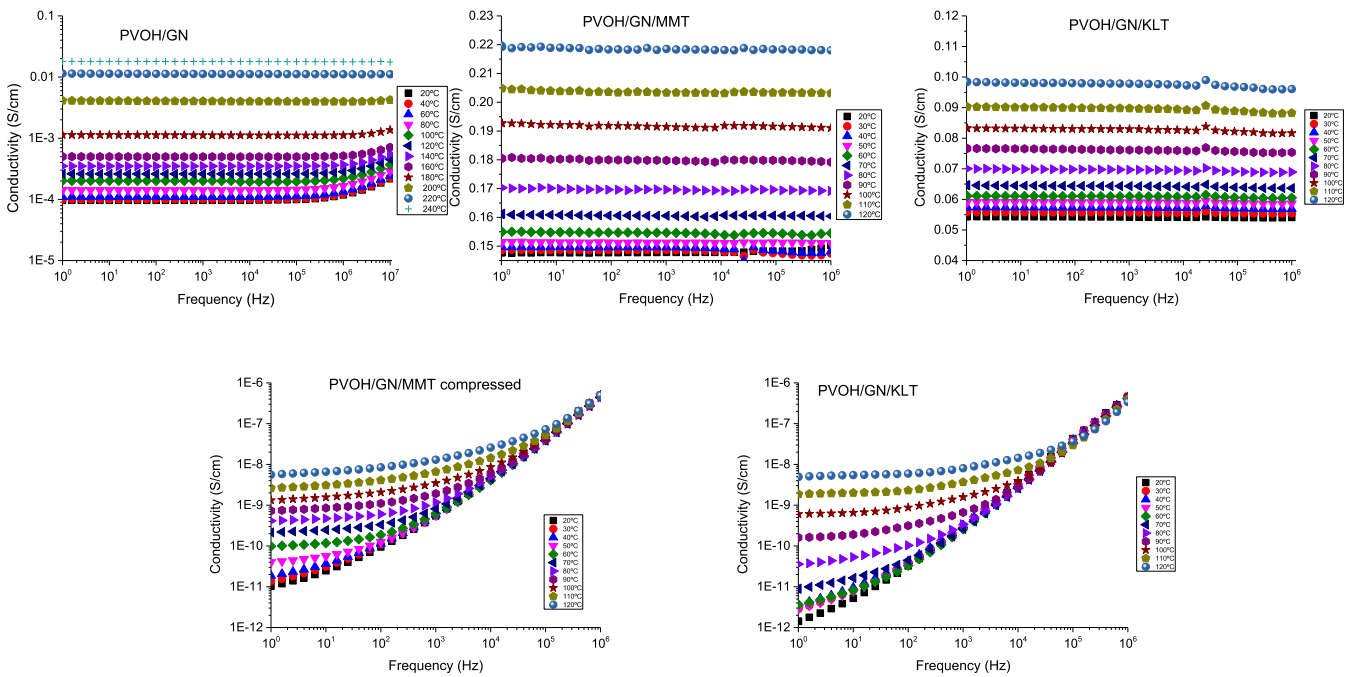

Figure 6. Conductivity vs frequency for the samples: (up) PVOH/GN, PVOH/GN/MMT, and PVOH/GN/KLT without compressed, and (bottom) PVOH/GN/MMT and PVOH/GN/KLT compressed, respectively, at different temperatures.

https://doi.org/10.1021/acsomega.2c05123
ACS Omega 2022, 7, 37954−37963

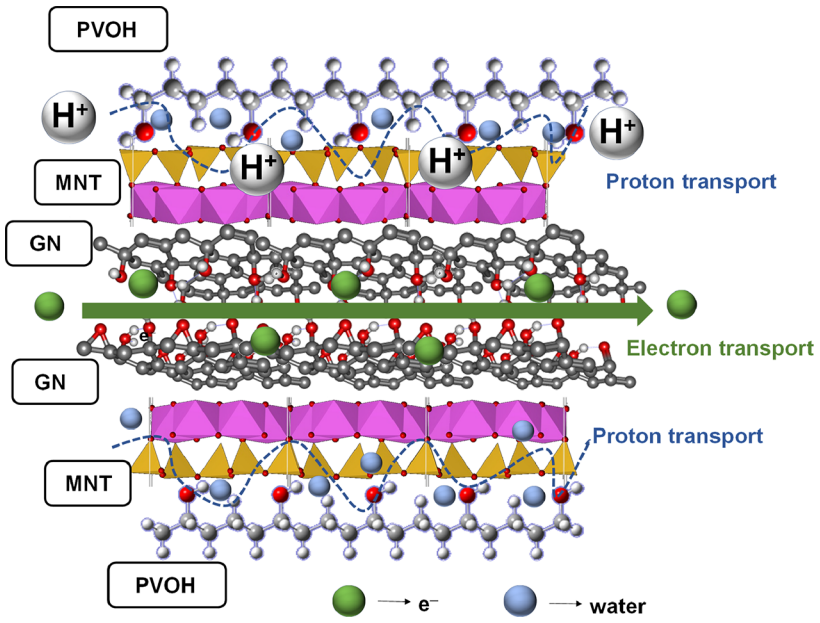

Figure 7. Schematic illustration of the dual electronic-ionic conductivity produced in the aerogels.

°C to 3.5×10^{-4}, 0.22 and 0.10 S/cm at 120 °C in the samples without compression of PVOH/GN, PVOH/GN/MMT, and PVOH/GN/KLT, respectively. On the other hand, for the samples PVOH/GN, the conductivities are significantly lower, around 3 orders of magnitude, than the samples with the incorporation of MMT. When increasing the temperature up to 240 °C, conductivity increased to 0.012 S/cm, which is 10-fold and 20-fold lower than PVOH/GN/KLT and PVOH/GN/MMT at only 120 °C, respectively. On the other hand, for the compressed samples, regardless of whether the clay is MMT or KLT, a capacitive behavior was observed, at least at low temperatures. From Figure 6 (bottom), it is clear that the aerogels have a capacitative response in the interval of temperatures between 20 and 80 °C, being the impedance directly proportional to the frequency with a slope around −1 and a correlation coefficient ca. 0.999 at low temperatures in the samples PVOH/GN/KLT and PVOH/GN/MMT, respectively. This is a field of study of great interest in the case of materials to use as electrolytes for capacitors and supercapacitors. It is worth mentioning that sample PVOH/GN has a great specific surface area to be configured as electrodes, which had a positive influence on the capacity and led to a reduction of the electrode resistance.[38] However, when the temperature increases up to 80 °C, the conductivity tends to a constant value in the region of low frequencies, that is, the sample behavior is conductive though with a very low conductivity such as observed in Figure 6. In addition, the differences in the conductivity can be rationalized to the different types of clay used in the aerogel preparation, MMT and KLT.

Finally, the difference in conductivity between uncompressed and compressed can be attributed to the fact that the charge conduction pathways have been blocked, as the lattice that facilitated transport through the GN and PVOH structures has been mostly destroyed. A comparison between our aerogel conductivities with single lithium-ion polymer electrolytes (SIPEs) permit us conclude that all our aerogels have conductivities more higher than the assumed values for practical use in Li-ion batteries, such is the case of different SIPEs with a suitable value lowest than 10^{-5} S/cm at room temperature.[39,40] Other poly-ionic liquids (PILs) such as Li-NTf_2 and Na-NTF_2 solutions in BMIN-TF_2 studied shown that the conductivity values of Li-NTf_2 solutions in the ILs 1,2-dimethyl-3-propylimidazolium bis(trifluoromethylsulfonyl)-imide (DMPI-NTF_2) and 1-ethyl-3-methylimidazolium bis-(trifluoromethylsulfonyl) imide (EMI-NTF_2) decrease with the increase of $LiNTF_2$, being the conductivities of 2.3 and 1.3 mS/cm, respectively, at 30 °C.[41] These values are 1 and 2 orders of magnitude smaller than our aerogels of PVOH/GN/KLT and PVOH/GN/MMT, respectively, at the same temperature. On the other hand, a comparison with the polymeric membrane based on polybenzimidazole (PBI) doped with 5 wt % GN, 3 wt % reduced GN oxide and 2 wt % of sulfonated GO showed conductivities of 0.27, 0.028, and 0.052 S/cm, measured at 180, 170, and 175 °C, respectively.[42,43] All of them are lower than the values found in our study for the aerogels at 120 °C.

In general, polymeric membranes containing ionic liquids (ILs) or PILs when bulk ILs have high ion densities and high mobility of their component ionic, as also observed in ionogel films based on mixtures of sulfonated zwitterionic salts and the ionic liquid Li-NTf_2, at different molar compositions, the conductivities observed can reach values around 10^{-2} S/cm above 100 °C,[44,45] smaller values than our aerogels. These results shows that the design of solid MMT/GN and KLT/GN composites as aerogels allows maximizing the space utilization of the electrode volume to achieve unhindered ion transport, which seems contrary to the general design principle of electrode materials where a suitable porous structure is desired, such as in our uncompressed samples. All this could be explained by admitting that GN oxide shows a dual electronic-ionic conductivity, such as shown in Figure 7, which acts not only as a pseudocapacitive filler for high-energy storage, as happens when we compress the samples, but also as a fast proton conductor. We hypothesize that the transport of protons is carried out along the interior of the dense microparticles when the compound is in the form of an aerogel. In particular, we support that the proton transport

https://doi.org/10.1021/acsomega.2c05123
ACS Omega 2022, 7, 37954−37963

process in most of the solid compound PVOH/GN/MMT or PVOH/GN/KLT depends on the distance between the charge and the hole, between which the jump is made and of the concentration of protons that we have, said process being similar to the process of diffusion of ions in a porous channel of a polymeric material. Similar results have been observed in polyaniline/GN composites by Xu et al.[46] However, our aerogels have conductivities 1 order of magnitude smaller than nitrogen-doped GN aerogel developed with dopamine (DA), although in this case, the conductivity was measured by the four-probe method with metal electrodes attached to the ends of cylindrical samples.[47]

In order to get more insights into the conduction mechanism, the activation energies for the ion diffusion process to occur within the aerogel have been determined. Figure 8 shows the variation of the conductivity with the

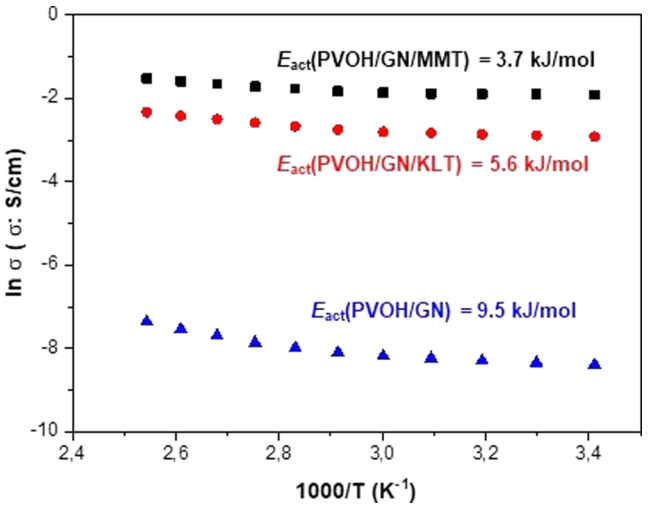

Figure 8. Reciprocal temperature dependence of conductivity of different samples: (black box solid) PVOH/GN/MMT, (red circle solid) PVOH/GN/KLT, and (blue triangle up solid) PVOH/GN.

temperature for the uncompressed samples PVOH/GN PVOH/GN/MMT and PVOH/GN/KLT, as a function of temperature. From the plot, we can observe that polymers with MMT as doping agents follow a typical Arrhenius behavior between 20 and 120 °C, where the tendency is linear for all ranges of temperature, where the conductivity increases when the temperature increases in accordance with Arrhenius eq 1. In the case of the PVOH/GN sample, the same behavior was observed but with a high diminution of the conductivity as a consequence of the change of doping agents, MMT by KLT.

$$\ln \sigma_{dc} = \ln \sigma_{\infty} - \frac{E_{act}}{RT} \quad (1)$$

From eq 1, the activation energy for each of the samples was calculated from the slopes by fitting the region 20−120 °C. The trend observed is as follows: E_{act}(PVOH/GN/MMT) kJ/mol < E_{act}(PVOH/GN/KLT) < E_{act}(PVOH/GN). However, in the case of PVOH/GN/KLT and PVOH/GN/MMT compressed, the activation energies were 165 and 86 kJ/mol, respectively. Our results show that all aerogels prepared display activation energies lower than most polymeric electrolytes which values depending on the polymer blend, which values generally vary between 10 and 25 kJ/mol. For example, thin films of PEO−GN oxide composites with $LiClO_4$/LiCl salts showed activation energies between 10 and 20 kJ/mol[48] and significantly smaller than the previous reported values for single lithium-ion polymer electrolytes based on poly(ionic liquids) in the same temperature ranges.[49]

The proton conductivity in PVOH/GN/MMT and PVOH/GN/KLT in all the range of temperatures studied is mainly given by a hydrogen bond pathway that builds a system of interconnected channels inside the framework. The low activation energies, (discussed further) characteristic of the Grotthus mechanism, support this assumption where the proton jumps through hydrogen bridges from PVOH. This observation not only confirms the need of interconnected channels for achieving the conductive behavior in the aerogels samples but also highlights the remarkably heterogeneous character in the surface of the samples cavities, which allows reaching the highest values of conductivity and low values of activation energy similar as happen in porous framework of divalent transition metal hexacyanocobaltates(III) where the anhydrous structure remains stable, preserving its porous features, up to 250 °C.[50]

This low activation energy values involve excellent ion mobilities through the lamellar structure such as observed in our aerogels. However, a rapid decrease in conductivity takes place when the samples are compressed due to the breaking of the ion pathways provided by the clays in union with the PVOH/GN structure. This may be due to the disposition of the clay, as an insulator, separating the ionic pathways provided by the PVOH together with the GN. Similar results have observed by Xia Wang and co-workers,[51] where superprotonic conduction through one-dimensional ordered alkali metal ion chains in a lanthanide-organic framework with conductivities of order of 10^{-2} S cm^{-1} (at 90 °C and 90% RH) and ultra-low activation energies of 0.1 eV, was determined. In the light of these results, porous solids of aerogels of PVOH/GN/MMT and PVOH/GN/KLT may be used as proton conductor materials to be used to build electrochemical devices as electrodes, sensors or batteries, and compressed can be used as capacitors.

CONCLUSIONS

In summary, innovative PVOH/GN/clay foamed systems have been successfully obtained. The mechanical properties of the polymer/clay aerogels are enhanced by incorporating GN into those systems. The addition of GN significantly increases its thermal stability, while the combination of PVOH and GN oxide produce interconnected channels to enhance the conductive when a clay (MMT or KLT) is added to the mixed PVOH/GN before to build the foam.

The design of solid MMT/GN and KLT/GN composites as aerogels allows maximizing the space utilization of the electrode volume to achieve unhindered ion transport, which seems contrary to the general design principle of electrode materials where a suitable porous structure is desired, such as in our uncompressed samples. All this could be explained by admitting that GN oxide shows a dual electronic-ionic conductivity, which acts not only as a pseudocapacitive filler for high-energy storage, as happens when we compress the samples, but also as a fast proton conductor. We think that the transport of protons is carried out along the interior of the dense microparticles when the compound is in the form of an aerogel. In particular, we have clearly shown that the proton transport process in most of the solid compound PVOH/GN/KLT or PVOH/GN/MMT depends on the distance between

https://doi.org/10.1021/acsomega.2c05123
ACS Omega 2022, 7, 37954−37963

the charge and the hole, between which the jump is made and of the concentration of protons that we have, said process being similar to the process of diffusion of ions in a porous channel of a polymeric material. This suggests that the proton conduction process in our aerogels is reminiscent of the Grotthuss mechanism, which together reveals an effective proton transportation pathway associated with aligned pathways built between the PVOH and GN oxide, such as observed by SEM and conductivity results. These promising results can extend the technological window of this type of materials to be used in electrodes, sensors, batteries, pressure-sensing applications, and supercapacitors.

AUTHOR INFORMATION

Corresponding Authors

Vicente Compañ − *Departamento de Termodinámica Aplicada (ETSII), Universitat Politècnica de València, 46022 Valencia, Spain;* orcid.org/0000-0001-8233-7472; Email: vicommo@ter.upv.es

Jose Gamez-Perez − *Departamento de Ingeniería de Sistemas Industriales y Diseño, Universitat Jaume I, Castellón de la Plana 12071, Spain*; Email: jose.gamez@esid.uji.es

Authors

Andreu Andrio − *Departamento de Física, Universitat Jaume I, Castellón de la Plana 12071, Spain*

Jorge Escorihuela − *Departamento de Química Orgánica, Universitat de València, 46100 Valencia, Spain;* orcid.org/0000-0001-6756-0991

Josua Velasco − *Departamento de Ingeniería de Sistemas Industriales y Diseño, Universitat Jaume I, Castellón de la Plana 12071, Spain*

Alejandro Porras-Vazquez − *Departamento de Ingeniería de Sistemas Industriales y Diseño, Universitat Jaume I, Castellón de la Plana 12071, Spain*

Complete contact information is available at: https://pubs.acs.org/10.1021/acsomega.2c05123

Author Contributions

The manuscript was written through contributions of all authors. All authors have given approval to the final version of the manuscript.

Funding

Financial support for this research from Ministerio de Economía y Competitividad (project AGL2015-63855-C2-2-R) (MINECO/FEDER) is gratefully acknowledged.

Notes

The authors declare no competing financial interest.

ACKNOWLEDGMENTS

The authors acknowledge the Servei Central d'Instrumentació Científica (SCIC-UJI) and Servei Central de Suport a la Investigació Experimental (SCSIE-UV) from Universitat Jaume I and Universitat de València, respectively, for the use of instruments and staff assistance. Authors would like to acknowledge José Ortega and Raquel Oliver for experimental support.

REFERENCES

(1) González, A.; Goikolea, E.; Barrena, J. A.; Mysyk, R. Review on supercapacitors: Technologies and materials. *Renewable Sustainable Energy Rev.* **2016**, *58*, 1189−1206.

(2) Yu, Z.; McInnis, M.; Calderon, J.; Seal, S.; Zhai, L.; Thomas, J. Functionalized graphene aerogel composites for high-performance asymmetric supercapacitors. *Nano Energy* **2015**, *11*, 611−620.

(3) Guan, L.; Yu, L.; Chen, G. Z. Capacitive and non-capacitive faradaic charge storage. *Electrochim. Acta* **2016**, *206*, 464−478.

(4) Nassar, G.; Daou, E.; Najjar, R.; Bassil, M.; Habchi, R. A review on the current research on graphene-based aerogels and their applications. *Carbon Trends* **2021**, *4*, 100065.

(5) Zhao, Z.; Moussa, M.; Shi, S.; Meng, Q.; Wang, R.; Ma, J. Compressible, electrically conductive, fibre-like, three-dimensional PEDOT-based composite aerogels towards energy storage applications. *Compos. Sci. Technol.* **2016**, *127*, 36−46.

(6) Basak, S.; Packirisamy, G. Graphene-Based Nanomaterials for Biomedical, Catalytic, and Energy Applications. *ChemistrySelect* **2021**, *6*, 9669−9683.

(7) Yu, Y.; De Andrade, L. C. X.; Fang, L.; Ma, J.; Zhang, W.; Tang, Y. Graphene oxide and hyperbranched polymer-toughened hydrogels with improved absorption properties and durability. *J. Mater. Sci.* **2015**, *50*, 3457−3466.

(8) Patra, S.; Munichandraiah, N. Supercapacitor studies of electrochemically deposited PEDOT on stainless steel substrate. *J. Appl. Polym. Sci.* **2007**, *106*, 1160−1171.

(9) Kistler, S. Coherent Expanded Aerogels and Jellies. *Nature* **1931**, *127*, 741.

(10) Cheng, Z.; DeGracia, K.; Schiraldi, D. A. Sustainable, Low Flammability, Mechanically-Strong Poly(vinyl alcohol) Aerogels. *Polymers* **2018**, *10*, 1102.

(11) Liu, L.; Wang, Y.; Alhassan, S. M.; Sun, H.; Choi, K.; Yu, C.; Schiraldi, D. A. Clay-Facilitated Aqueous Dispersion of Graphite and Poly(vinyl alcohol) Aerogels Filled with Binary Nanofillers. *Gels* **2018**, *4*, 8.

(12) Matsumura, S.; Kurita, H.; Shimokobe, H. Anaerobic biodegradability of polyvinyl alcohol. *Biotechnol. Lett.* **1993**, *15*, 749−754.

(13) Li, X.; Guo, M.; Bandyopadhyay, P.; Lan, Q.; Xie, H.; Liu, G.; Liu, X.; Cheng, X.; Kim, N. H.; Lee, J. H. Two-dimensional materials modified layered double hydroxides: A series of fillers for improving gas barrier and permselectivity of poly(vinyl alcohol). *Composites, Part B* **2021**, *207*, 108568.

(14) Simón-Herrero, C.; Peco, N.; Romero, A.; Valverde, J. L.; Sánchez-Silva, L. PVA/nanoclay/graphene oxide aerogels with enhanced sound absorption properties. *Appl. Acoust.* **2019**, *156*, 40−45.

(15) Rapisarda, M.; Malfense Fierro, G. P.; Meo, M. Ultralight graphene oxide/polyvinyl alcohol aerogel for broadband and tuneable acoustic properties. *Sci. Rep.* **2021**, *11*, 10572.

(16) Li, C.; Li, Y.; She, X.; Vongsvivut, J.; Li, J.; She, F.; Gao, W.; Kong, L. Reinforcement and deformation behaviors of polyvinyl alcohol/graphene/montmorillonite clay composites. *Compos. Sci. Technol.* **2015**, *118*, 1−8.

(17) Ahmed, M.; Thithai, S.; Weon, V.; Weon, C. J. Production and characteristic features of lignin-PVA aerogels for oil spillage applications. *Mater. Chem. Phys.* **2022**, *289*, 126455.

(18) Díez, I.; Eronen, P.; Österberg, M.; Linder, M. B.; Ikkala, O.; Ras, R. H. A. Functionalization of Nanofibrillated Cellulose with Silver Nanoclusters: Fluorescence and Antibacterial Activity. *Macromol. Biosci.* **2011**, *11*, 1185−1191.

(19) Zheng, Q.; Cai, Z.; Gong, S. Green synthesis of polyvinyl alcohol (PVA)-cellulose nanofibril (CNF) hybrid aerogels and their use as superabsorbents. *J. Mater. Chem. A* **2014**, *2*, 3110−3118.

(20) Sun, Y.; Li, D.; Kim, J. U.; Li, B.; Cho, S. H.; il Kim, T.; Do Nam, J.; Ci, L.; Suhr, J. Carbon aerogel reinforced PDMS nanocomposites with controllable and hierarchical microstructures for multifunctional wearable devices. *Carbon* **2020**, *171*, 758−767.

(21) Tewari, A.; Gandla, S.; Bohm, S.; McNeill, C. R.; Gupta, D. Highly Exfoliated MWNT-rGO Ink-Wrapped Polyurethane Foam for Piezoresistive Pressure Sensor Applications. *ACS Appl. Mater. Interfaces* **2018**, *10*, 5185−5195.

(22) Cheng, Z.-H.; Guo, M.-L.; Chen, X.-Y.; Wang, T.; Wang, Y.-Z.; Schiraldi, D. A. Reduction of PVA Aerogel Flammability by Incorporation of an Alkaline Catalyst. *Gels* **2021**, *7*, 57.
(23) Yan, S.; Song, H.; Li, Y.; Yang, J.; Jia, X.; Wang, S.; Yang, X. Integrated reduced graphene oxide/polypyrrole hybrid aerogels for simultaneous photocatalytic decontamination and water evaporation. *Appl. Catal., B* **2022**, *301*, 120820.
(24) Zhu, T.; Zhou, C.; Kabwe, F.; Wu, Q.; Li, C.; Zhang, J. Exfoliation of montmorillonite and related properties of clay/polymer nanocomposites. *Appl. Clay Sci.* **2019**, *169*, 48−66.
(25) Chen, T.; Yuan, Y.; Zhao, Y.; Rao, Y.; Song, F.; Song, S. Effect of layer charges on exfoliation of montmorillonite in aqueous solutions. *Colloids Surf., A* **2018**, *548*, 92−97.
(26) Madyan, O. A.; Fan, M.; Feo, L.; Hui, D. Physical properties of clay aerogel composites: An overview. *Composites, Part B* **2016**, *102*, 29−37.
(27) Fuentes, I.; Andrio, A.; García-Bernabé, A.; Escorihuela, J.; Viñas, C.; Teixidor, F.; Compañ, V. Structural and dielectric properties of cobaltacarborane composite polybenzimidazole membranes as solid polymer electrolytes at high temperature. *Phys. Chem. Chem. Phys.* **2018**, *20*, 10173−10184.
(28) Barjola, A.; Escorihuela, J.; Andrio, A.; Giménez, E.; Compañ, V. Enhanced Conductivity of Composite Membranes Based on Sulfonated Poly(Ether Ether Ketone) (SPEEK) with Zeolitic Imidazolate Frameworks (ZIFs). *Nanomaterials* **2018**, *8*, 1042.
(29) Viot, P.; Beani, F.; Lataillade, J. L. Polymeric foam behavior under dynamic compressive loading. *J. Mater. Sci.* **2005**, *40*, 5829−5837.
(30) Alasfar, R. H.; Ahzi, S.; Barth, N.; Kochkodan, V.; Khraisheh, M.; Koç, M. A Review on the Modeling of the Elastic Modulus and Yield Stress of Polymers and Polymer Nanocomposites: Effect of Temperature, Loading Rate and Porosity. *Polymers* **2022**, *14*, 360.
(31) Gorgolis, G.; Galiotis, C. Graphene aerogels: a review. *2D Mater.* **2017**, *4*, 032001.
(32) Wang, Y.; Gawryla, M. D.; Schiraldi, D. A. Effects of freezing conditions on the morphology and mechanical properties of clay and polymer/clay aerogels. *J. Appl. Polym. Sci.* **2013**, *129*, 1637−1641.
(33) Yi, H.; Xia, L.; Song, S. Three-dimensional montmorillonite/Ag nanowire aerogel supported stearic acid as composite phase change materials for superior solar-thermal energy harvesting and storage. *Compos. Sci. Technol.* **2022**, *217*, 109121.
(34) Zhang, X.; Wang, J.; Wang, L.; Li, Z.; Wang, R.; Li, H.; Luo, M.; Liu, H.; Hu, W.; Feng, Q. Effects of kaolinite and its thermal transformation on oxidation of heavy oil. *Appl. Clay Sci.* **2022**, *223*, 106507.
(35) Holland, B. J.; Hay, J. N. The thermal degradation of poly(vinyl alcohol). *Polymer* **2001**, *42*, 6775−6783.
(36) Fan, D.; Yang, X.; Liu, J.; Zhou, P.; Zhang, X. Highly aligned graphene/biomass composite aerogels with anisotropic properties for strain sensing. *Compos. Commun.* **2021**, *27*, 100887.
(37) Wei, S.; Qiu, X.; An, J.; Chen, Z.; Zhang, X. Highly sensitive, flexible, green synthesized graphene/biomass aerogels for pressure sensing application. *Compos. Sci. Technol.* **2021**, *207*, 108730.
(38) Katakabe, T.; Kaneko, T.; Watanabe, M.; Fukushima, T.; Aida, T. Electric Double-Layer Capacitors Using "Bucky Gels" Consisting of an Ionic Liquid and Carbon Nanotubes. *J. Electrochem. Soc.* **2005**, *152*, A1913.
(39) Yu, Y.; Lu, F.; Sun, N.; Wu, A.; Pan, W.; Zheng, L. Single lithium-ion polymer electrolytes based on poly(ionic liquid)s for lithium-ion batteries. *Soft Matter* **2018**, *14*, 6313−6319.
(40) Meziane, R.; Bonnet, J.-P.; Courty, M.; Djellab, K.; Armand, M. Single-ion polymer electrolytes based on a delocalized polyanion for lithium batteries. *Electrochim. Acta* **2011**, *57*, 14−19.
(41) Seki, S.; Ohno, Y.; Kobayashi, Y.; Miyashiro, H.; Usami, A.; Mita, Y.; Tokuda, H.; Watanabe, M.; Hayamizu, K.; Tsuzuki, S.; Hattori, M.; Terada, N. Imidazolium-Based Room-Temperature Ionic Liquid for Lithium Secondary Batteries. *J. Electrochem. Soc.* **2007**, *154*, A173−A177.
(42) Üregen, N.; Pehlivanoğlu, K.; Özdemir, Y.; Devrim, Y. Development of polybenzimidazole/graphene oxide composite membranes for high temperature PEM fuel cells. *Int. J. Hydrogen Energy* **2017**, *42*, 2636−2647.
(43) Xu, C.; Cao, Y.; Kumar, R.; Wu, X.; Wang, X.; Scott, K. A polybenzimidazole/sulfonated graphite oxide composite membrane for high temperature polymer electrolyte membrane fuel cells. *J. Mater. Chem.* **2011**, *21*, 11359−11364.
(44) Valverde, D.; Garcia-Bernabé, A.; Andrio, A.; García-Verdugo, E.; Luis, S. V.; Compañ, V. Free ion diffusivity and charge concentration on cross-linked polymeric ionic liquid iongel films based on sulfonated zwitterionic salts and lithium ions. *Phys. Chem. Chem. Phys.* **2019**, *21*, 17923−17932.
(45) Compañ, V.; Escorihuela, J.; Olvera, J.; García-Bernabé, A.; Andrio, A. Influence of the anion on diffusivity and mobility of iònic liquids composite polybenzimidazol membranes. *Electrochim. Acta* **2020**, *354*, 136666.
(46) Xu, Y.; Tao, Y.; Li, H.; Zhang, C.; Liu, D.; Qi, C.; Luo, J.; Kang, F.; Yang, Q.-H. Dual electronic-ionic conductivity of pseudocapacitive filler enables high volumetric capacitance from dense graphene micro-particles. *Nano Energy* **2017**, *36*, 349−355.
(47) Song, X.; Lin, L.; Rong, M.; Wang, Y.; Xie, Z.; Chen, X. Mussel-inspired, ultralight, multifunctional 3D nitrogen-doped graphene aerogel. *Carbon* **2014**, *80*, 174−182.
(48) Khan, M. S.; Shakoor, A. Ionic Conductance, Thermal and Morphological Behavior of PEO-Graphene Oxide-Salts Composites. *J. Chem.* **2015**, *2015*, 695930.
(49) Yu, Y.; Lu, F.; Sun, N.; Wu, A.; Pan, W.; Zheng, L. Single lithium-ion polymer electrolytes based on poly(ionic liquid)s for lithium-ion batteries. *Soft Matter* **2018**, *14*, 6313−6319.
(50) Roque, J. R.; Reguera, E.; Balmaseda, J.; Rodríguez-Hernández, J.; Reguera, L.; del Castillo, L. F. Porous hexacyanocobaltates(III): Role of the metal on the framework properties. *Microporous Mesoporous Mater.* **2007**, *103*, 57−71.
(51) Wang, X.; Wang, Y.; Silver, M. A.; Gui, D.; Bai, Z.; Wang, Y.; Liu, W.; Chen, L.; Diwu, J.; Chai, Z.; Wang, S. Superprotonic conduction through one-dimensional ordered alkali metal ion chains in a lanthanide-organic framework. *Chem. Commun.* **2018**, *54*, 4429−4432.

https://doi.org/10.1021/acsomega.2c05123
ACS Omega 2022, 7, 37954−37963